ACS OMEGA

Open Access

http://pubs.acs.org/journal/acsodf

Article

Mechanical Reliability and Biocompatibility of Graphene-Modified Photocurable Resins for Additive Manufacturing: Implications for Potential Biomedical Use

Sara Lopez de Armentia,* Victor Manuel Villapún, Yolanda Ballesteros, Juan Carlos del Real, Lucy Arkinstall, Sophie Constance Cox, Nicholas Dunne, and Eva Paz

Cite This: *ACS Omega* 2026, 11, 20489−20499

Read Online

ACCESS | Metrics & More | Article Recommendations

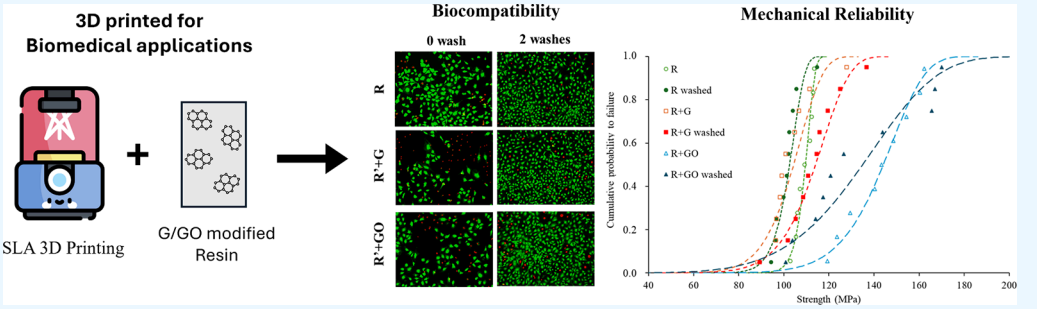

ABSTRACT: Additive manufacturing using stereolithography enables the fabrication of intricate small-scale parts, making it ideal for biomedical applications such as prostheses and scaffolds. This study evaluates the mechanical reliability and biocompatibility of photocurable acrylic resins modified with graphene-based nanomaterials, graphene (G) and graphene oxide (GO), to address limitations in their use for biomedical products, where high reliability and predictable performance under mechanical stress are critical to ensuring safety and functionality. Through mechanical testing and Weibull distribution modeling, it was found that GO significantly enhances the characteristic strength (σ_θ) of the resin, improving its performance under mechanical stress; however, the reliability of this strength decreased as evidenced by a reduction in the Weibull modulus (m). Postprinting washing, aimed at reducing cytotoxic leaching, improved biocompatibility with cell viability exceeding 90%, though it slightly decreased the compression strength and increased the variability. GO-modified resins exhibited enhanced mechanical and biocompatibility profiles compared to G-modified resins, which showed limited interaction with the resin matrix. These findings offer important insights for optimizing mechanical reliability and biocompatibility, advancing the development of materials suitable for safe and reliable human-body contact in regenerative medicine.

1. INTRODUCTION

In modern biomedical engineering, the development of functional and biocompatible materials has significantly advanced tissue engineering and regenerative medicine.[1−3] Additive manufacturing techniques, particularly stereolithography (SLA), have emerged as promising solutions for diverse applications, including the creation of patient-specific surgical guides, educational models, prostheses, implants, and scaffolds. These applications demand precise geometries, biocompatibility, and mechanical reliability, making SLA ideal for fabricating complex devices with exceptional resolution (10−150 μm) and intricate precision.[4]

In the context of bone regeneration, SLA is particularly interesting in fabricating scaffolds that mimic the intricate structure and mechanical properties of natural bone tissue, making them potential substitutes for bone autografts.[5,6] These scaffolds typically feature controlled porosity and pore sizes (100−500 μm), enhancing cell attachment, vascularization, and subsequent regeneration.[7,8] Furthermore, SLA facilitates the manufacture of custom implants and prostheses tailored to patient-specific anatomical requirements, incorporating lattice scaffolds to promote osteointegration and reduce implant stiffness, thus improving compatibility with natural bone mechanics.[9−11] While these advancements address structural and functional demands, achieving an optimal combination of biocompatibility and mechanical performance remains a critical factor for long-term orthopedic applications.

Received: November 11, 2025
Revised: March 9, 2026
Accepted: March 18, 2026
Published: March 28, 2026

SLA primarily relies on photocurable polymeric resins as the base material, with acrylic formulations being the most widely used due to their excellent versatility, mechanical properties, and ease of processing. To enhance the performance of these materials, researchers have increasingly focused on reinforcing acrylic polymers with graphene-based nanomaterials (GBN), such as graphene (G) and graphene oxide (GO). These nanomaterials have shown significant potential to improve the mechanical strength, durability, and biological functionality of resins.[12−14] Specifically, GBN has been demonstrated to promote cell adhesion and proliferation,[15] reduce pro-inflammatory immune responses,[16] and exhibit antibacterial properties,[17] making them particularly interesting for biomedical applications. This integration represents a transformative approach, enabling the creation of scaffolds with enhanced mechanical integrity and biological functionality.

Despite extensive studies on the mechanical reinforcement properties of GBN composites, concerns persist regarding the potential cytotoxic effects of GBN and residual monomers in photocurable resins. The dose-dependent risks associated with introducing these nanomaterials into the human body remain a critical area of investigation, with conflicting results reported in the literature.[18−20] In addition to GBN-related cytotoxicity, acrylic polymers exhibit limitations regarding biological performance due to residual monomers remaining after polymerization. These residual monomers and unreacted photoinitiators, known to leach from the material, cause oxidative stress, enzymatic inhibition, and interactions with cell membranes, negatively impacting biocompatibility and safety.[21,22] Consequently, the adoption of SLA technology is predominantly restricted to short-term applications in tissues, bones, dentin, and mucosal membranes. Only in specific cases, such as skin-contact scenarios compliant with USP Class VI certification, has its use been extended to longer durations.[23] Understanding the toxicological effects of these composite materials is thus imperative for ensuring their safe and effective long-term use in biomedical applications.

Recent research has focused on addressing these challenges, emphasizing the need to expand SLA applications for longer-term and more intimate interactions with the human body. Enhancing the biocompatibility of acrylic resins is a crucial step toward unlocking the full potential of SLA for diverse medical applications.[24] To address these concerns, methods such as warm water immersion, ultrasonic cleaning,[25−27] microwaving,[27] and autoclaving[28] have been proposed. For 3D-printed resins, washing and postcuring methods have shown promise in reducing the leaching of toxic substances, thereby improving cell viability resins.[29]

Additionally, beyond biocompatibility, reliability is a key factor for ensuring the success of materials intended for long-term biomedical applications, where consistent performance under diverse conditions is critical to maintaining safety and functionality. While many studies have explored the mechanical reinforcement potential of GBN in resins, the broader implications for the reliability of these materials remain underexplored. Mechanical strength alone is insufficient to fully evaluate its applicability in real-world biomedical applications. In such applications, materials must perform consistently and predictably to ensure patient safety and the long-term functionality of medical devices such as prostheses and scaffolds, where any failure could have serious consequences for patient health and quality of life. Weibull analysis, widely used in the evaluation of reliability in orthopedic and other medical materials, offers a powerful tool to assess the variability and predictability of mechanical performance.[30,31] By analyzing the Weibull modulus (m) and characteristic strength (σ_θ), it is possible to evaluate not only the material's strength but also its reliability and consistency, providing deeper insights into its suitability for load-bearing and long-term applications.

This study combines Weibull analysis with biocompatibility assessments to evaluate the performance of GBN-modified resins for additive manufacturing. By emphasizing the critical importance of reliability alongside mechanical strength, this work provides insights necessary for the safe and effective use of these materials in biomedical applications such as prosthetics and scaffolds. The approach advances the understanding of GBN-modified resins, optimizing SLA-fabricated materials for practical healthcare applications requiring consistent and predictable performance.

2. EXPERIMENTAL METHODOLOGY

2.1. Materials

The resin used for SLA was a commercial photocurable acrylic-based resin Formlabs Clear FLGPCL4 (Formlabs, Somerville, MA, USA), which for clarity purposes will be referred to as R. As reinforcement, graphene, G (Avanzare Nanotechnology, La Rioja, Spain), and graphene oxide, GO (NanoInnova Technologies, Toledo, Spain), were used with an average lateral size of 2−4 μm and 4−8 μm and a sheet thickness between 1 and 2 sheets and 0.7−1.2 nm, respectively.

2.2. Sample Preparation

Nanocomposites were prepared following the procedure explained in ref 32. Briefly, 0.05 wt % of the GBN was dispersed in MMA via probe sonication (Branson 450, Branson Ultrasonics Corp., CT, USA) with resin added at different sonication stages. After the dispersion, a degassing process was carried out in an ultrasonic bath followed by a vacuum process in an oven (<0.1 atm at room temperature).

To analyze the effect of the addition of MMA, R′ samples were manufactured. They were prepared following the same procedure explained in the previous paragraph but without the addition of GBN and an R:MMA ratio of 300:10 v/v.

Acrylic resin samples were printed with an SLA printer Form 2 (Formlabs, Somerville, MA, USA). The layer thickness was set at 100 μm, and the exposure time was optimized depending on the loaded sample.[33] For that reason, the R+G sample exposure time was increased by 8.9% from the manufacturer's recommendations on pure R.

After printing, samples were cleaned with isopropyl alcohol (IPA) in a FormWash (Formlabs, Somerville, MA, USA) equipment for 3 min. In addition, they were subjected to a postcuring process in a FormCure chamber (Formlabs, Somerville, MA, USA) for 90 min at 80 °C.

Images of the printed samples take were shown in Figure 1.

To analyze the mechanical and biological behavior of the unwashed and washed samples, three different types of samples were manufactured.

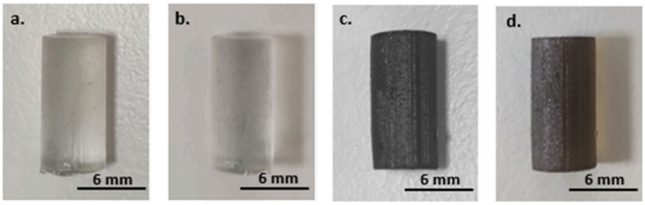

Figure 1. Images of printed R (a), R′ (b), R′ + G (c), and R′ + GO (d).

https://doi.org/10.1021/acsomega.5c11858
ACS Omega 2026, 11, 20489−20499

- Cylindrical-shaped samples with a diameter of 6 mm and 12 mm height for compression tests.
- Rectangular parallelepiped-shaped samples of 8 × 4 × 15 mm for hardness and water absorption assays.
- Disc-shaped samples with a diameter of 10 mm and 4 mm height for elution and cell analysis.

2.3. Experimental Procedure

2.3.1. Biological Evaluation. To analyze the potential effect of the selected resin, nanofillers and possible routes to diminish toxicity, leaching components were collected and used on a preseeded mouse osteoblastic precursor cell line (MC3T3-E1 Subclone 1, ATCC CRL-2593, P26−28). For eluent collection, samples were cleaned by immersion and sonication in industrial methylated spirit (IMS) 70% for 10 min, followed by sterilization through UV light exposure for 20 min. Next, samples were immersed in fresh basal media (Dulbecco's Modified Eagle's Medium supplemented with 10% fetal bovine serum, 1% penicillin/streptomycin and 0.5 g/L L-glutamine, all of them supplied by Sigma-Aldrich, St. Louis, MS, USA) for 24, 48, 72 h or 7 days at room temperature.

For the washing experiments, sterilized samples were pretreated by immersion in basal media for 24 and 48 h, replacing the media each day. In this section, resin with MMA (R′) was also analyzed together with the other composites to discern if the possible effect on biological testing was due to the addition of GBN or MMA.

Before testing, 5,000 cells/well were seeded in a 96 well-plate and incubated for 24 h at 37 °C and 5% CO_2 with fresh basal media. Then, the aforementioned eluents were used to replace the nutrient media and recultivated as necessary followed by Live/Dead staining using 100 μL of a calcein-AM and PI solution (1.5 μL of calcein-AM and 10 μL of PI in 1 mL of DPBS) per well. After incubation at 37 °C and 5% CO_2 images were taken with a fluorescence microscope system (EVOS M5000, Thermo Scientific). Cells treated with fresh media were used as positive controls in all tests. A quantitative analysis was carried out to calculate the coverage of green and red channels with ImageJ 1.35 software. At least three images were analyzed for each sample.

2.3.2. Nuclear Magnetic Resonance (NMR). Before analysis, all samples were left in deuterated water (D_2O) for at least 24 h before testing on an Avance-NEO-400 (Bruker, UK) spectrometer in D_2O at 298 K. All liquid-state NMR spectra were referenced to the residual solvent peak, 4.790 ppm in D_2O. To analyze them, it is important to denote the characteristic peaks of the most likely components (MMA and TPO) to elute. The MMA spectrum is characterized by intense peaks appearing at 6.10, 5.55, 3.75, and 1.95 ppm, corresponding to the A, B, C and D hydrogens (Figure 2a).[34] The exact acrylate

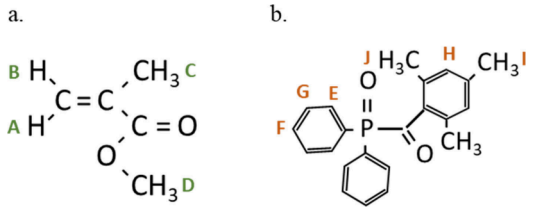

Figure 2. Depiction of (a) MMA and (b) TPO molecules including characteristic bonds for their identification in ^1H NMR spectra.

monomers of the commercial resin are not completely known; however, the A, B and D hydrogens are common to all acrylate monomers, facilitating monomer detection. Conversely, the characteristic peaks of TPO reduce at 7.99, 7.55, 7.50, 6.80, 2.25, and 2.03 ppm for E to J hydrogens (Figure 2b).[35]

2.3.3. Mechanical Testing. Compression tests were conducted in both unwashed and optimally washed samples using a Universal Testing Machine IBTH/500 (Ibertest, Madrid, Spain) with a load cell of 5 kN. Compression tests were carried out at a rate of 20 mm/min with at least 10 samples per condition analyzed.

Shore D hardness was measured on five samples per condition with a Shore D hardness tester (Bareiss GmbH, Berlin, Germany) applying 50 N, following standard UNE-EN ISO 868.

For both compression and hardness measurements, washed samples were tested after 1 h of drying at room temperature.

2.3.4. Water Absorption. Changes in sample weight before washing and after two washing cycles of 24 h were measured. The as-manufactured sample was used as a reference. Measurements were conducted using an analytical balance (precision 0.1 mg) after 1 h of drying and after complete drying at 35 °C. The evaluation of complete drying involved weighing the sample daily until three consecutive measurements exhibited a change of less than 0.1 mg. At least five samples per condition were measured.

2.3.5. Fracture Analysis. Field emission scanning electron microscopy (FESEM) was used to investigate the fracture mechanisms and microstructural features of the samples cryo-fractured in liquid nitrogen. A TENEO-LoVac instrument (Eindhoven, Netherlands) was used. Before imaging, the samples were prepared by cryogenic fracturing in liquid nitrogen to preserve the inherent fracture characteristics. Following fracturing, the samples were sputter-coated with a thin layer of gold to enhance conductivity and improve image clarity.

2.3.6. Statistical Analysis. One-way analysis of variance (ANOVA) test with a post hoc Scheffe's test was used to evaluate the results for statistical significance with the software SPSS 28.0 for Windows (IBM SPSS, Chicago, IL, USA). A p-value lower than 0.05 was indicative of statistical significance.

To assess the variability and reliability of material strength, a two-parameter Weibull distribution was applied, as it is particularly suited for analyzing materials and mechanical systems with high variability in strength properties. The compressive strength data obtained from the mechanical tests were evaluated using this distribution to characterize the failure behavior of the reinforced resin materials. The Weibull cumulative distribution function is defined as

$$P_f = 1 - \exp\left[-\left(\frac{\sigma}{\sigma_\theta}\right)^m\right] \quad (1)$$

where P_f represents the cumulative probability of failure; σ is the measured compression strength; σ_θ is the characteristic compression strength (the scale parameter); and m is the Weibull modulus (shape parameter). The characteristic strength, σ_θ, corresponds to the stress level at which there is a 63.2% probability of failure, serving as a critical benchmark for evaluating material reliability. At this stress level, 63.2% of the samples are expected to fail, while the remaining samples exceed this strength.

The Weibull modulus, m, provides insights into the variability of the strength results. A higher m value indicates less dispersion in the strength data, reflecting greater consistency and predictability in the material's mechanical performance.

A statistical fit of the experimental compressive strength data to the two-parameter Weibull distribution was performed using the maximum likelihood estimation (MLE) method, implemented via a custom Python script using SciPy library.[36] This approach enables accurate estimation of the Weibull parameters by directly maximizing the likelihood function.

In contrast to conventional approaches often used in Weibull parameter estimation—such as graphical methods based on linear regression of transformed data and empirical plotting position formulas like Bernard's or Hazen approximations—the MLE method does not require prior assumptions about the cumulative failure probability of each data point. This results in a more objective and statistically rigorous analysis, which is particularly advantageous when working with small sample sizes or data sets with high variability.

Confidence intervals for the characteristic strength were calculated using the chi-squared distribution, while uncertainty in the Weibull modulus was assessed through classical approaches such as Fisher information or profile likelihood methods.

To complement the numerical fitting, cumulative probability of failure plots were generated for each material. In these plots, the

https://doi.org/10.1021/acsomega.5c11858
ACS Omega 2026, 11, 20489−20499

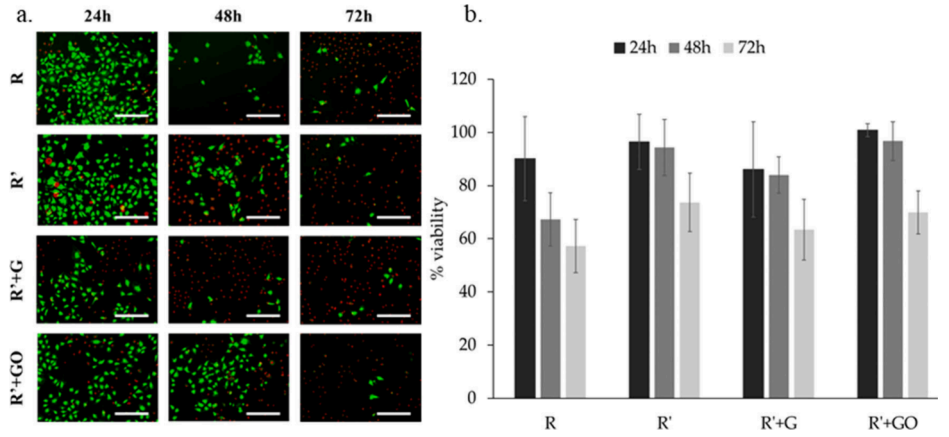

Figure 3. MC3T3-E1 cells exposed to eluents collected after 24, 48, and 72 h in contact with R and its composites. (a) Live/Dead micrographs (scale bar 300 μm) and (b) quantitative cell viability.

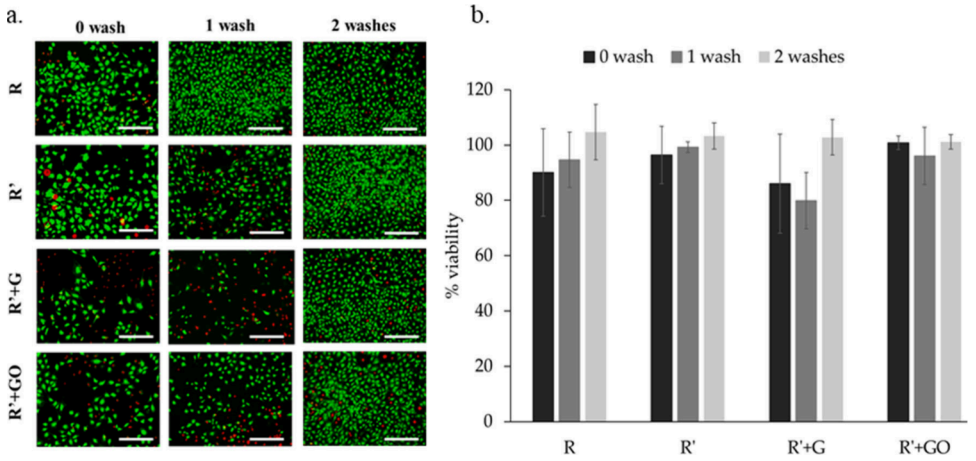

Figure 4. MC3T3-E1 cells exposed to eluents collected after 24 h in contact with R and its composites after 0, 1, and 2 washes. (a) Live/Dead micrographs (scale bar 300 μm) and (b) quantitative cell viability.

experimental data points were assigned failure probabilities using the empirical formula (eq 2)

$$P_f = \frac{i - 0.5}{N} \quad (2)$$

where i is the rank of the ordered strength value and N is the total number of observations. This method, known as the Hazen approximation, is commonly used in Weibull analysis to estimate empirical cumulative failure probabilities based on ranked data. It provides a practical visual reference of the experimental behavior without assuming an underlying distribution. These empirical points were plotted alongside the theoretical Weibull distribution curves obtained through maximum likelihood estimation (MLE), enabling a direct visual comparison between the observed data and the model-predicted failure behavior.

3. RESULTS

3.1. Cytotoxicity

Cells were cultured with eluents collected after 24, 48, and 72 h of contact with the resin to assess the cytotoxicity of sample extracts with Live/Dead staining (Figure 3). The base resin, R, demonstrated high levels of cytotoxicity following 48 and 72 h of elution (68.2% and 57.6% of viability, respectively), suggesting the presence of residual monomer or other toxic constituents that were released into the medium after 48 h. Notably, the modified resin, R′, which includes additional MMA, exhibited higher cell viability compared to R (93.1% and 72.2% after 48 and 72 h, respectively). This result indicates that the increased MMA content, used for GBN dispersion, does not negatively affect cytotoxicity.

When comparing the GBN samples (R′ + G and R′ + GO) to R, there was a variation between nanofiller with G showing increased toxicity (86.1% of cell viability) after 24 h of elution compared to the marginally better results of the resin loaded with GO (100.6%).

To assess the possibility of removing these toxic eluents, the leachable from washed samples was collected and used on preseeded MC3T3 cells (Figure 4). These images showed similar toxicity levels in the unwashed controls as previously observed, albeit a clear reduction in cells displaying membrane damage and an increase in metabolically active cells can be noticed after washing. This effect is dependent on washing times and material tested with R, R′, and R′ + GO requiring a single processing step while R′ + G necessitated two washing cycles to enable cell survival. The observed reduction in cytotoxicity after two 24-h washing cycles suggests that leachable residual monomers and/or photoinitiator-related species are effectively removed during this process. It can be hypothesized that this reduction may be primarily attributed to diffusion-driven extraction into the culture medium, potentially aided by interactions with serum proteins present in the medium. Cell viability is increased by a 17.2% when R was

https://doi.org/10.1021/acsomega.5c11858
ACS Omega 2026, 11, 20489−20499

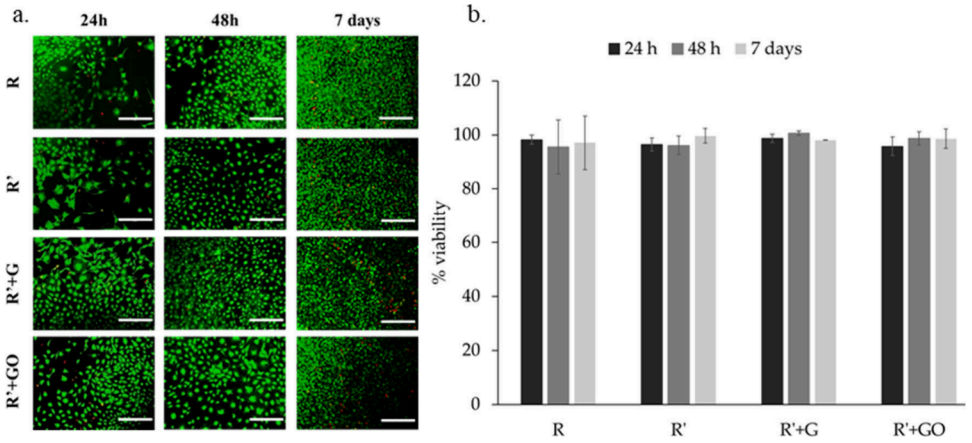

Figure 5. MC3T3-E1 cells were exposed 24 h, 48 h, and 7 days to eluents collected after 7 days in contact with washed samples. (a) Live/Dead micrographs (scale bar 300 μm) and (b) quantitative cell viability.

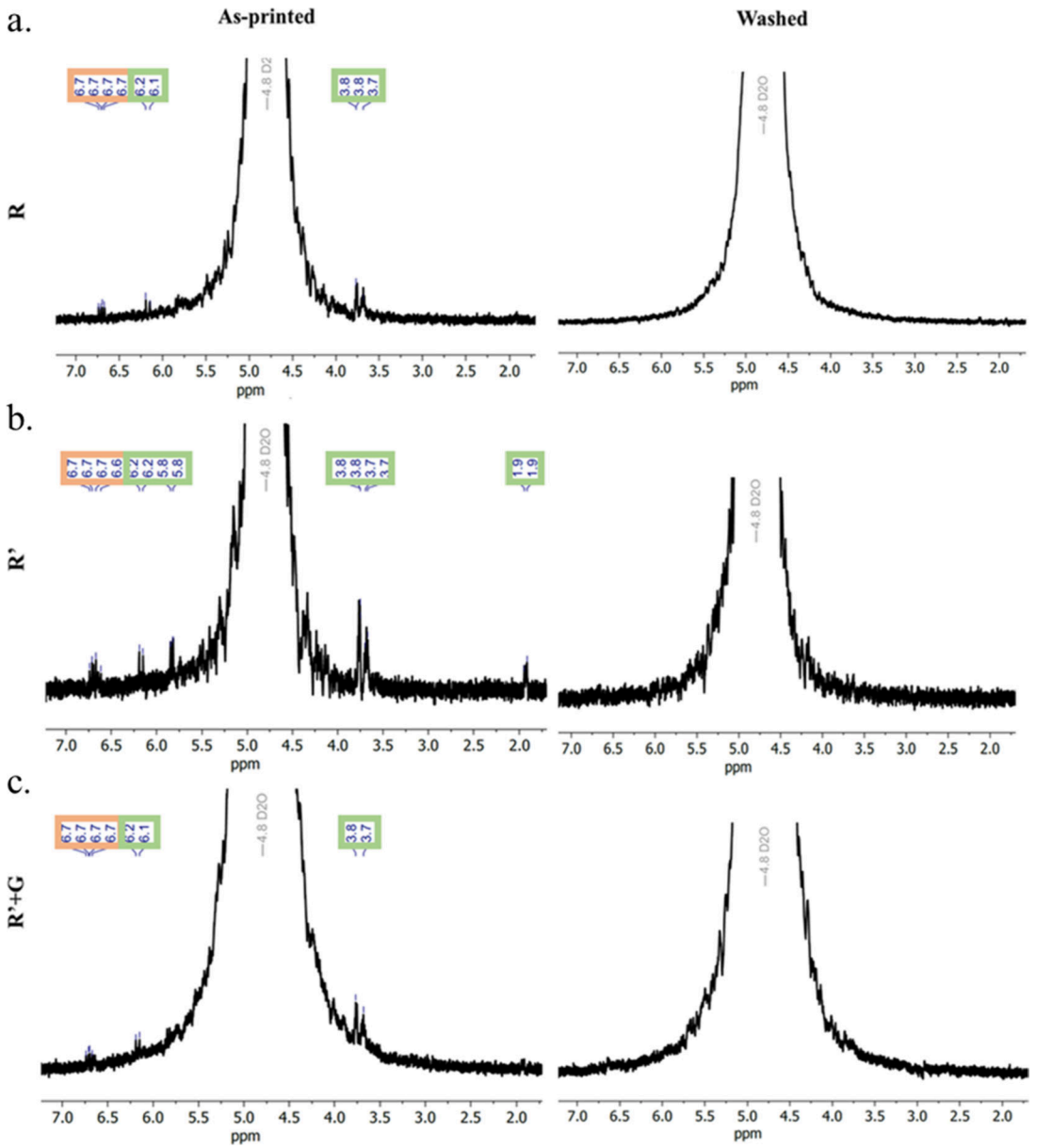

Figure 6. NMR spectrum of unwashed and washed (a) R, (b) R′, and (c) R′ + G. Peaks boxed in green are due to MMA and in orange are due to TPO.

https://doi.org/10.1021/acsomega.5c11858
ACS Omega 2026, 11, 20489−20499

Table 1. Shore D Hardness and Weight Change of As-Printed, Washed and Washed + Dried Samples[a]

		R	R′ + G	R′ + GO
As-printed	Shore D hardness	81 ± 3[a]	78 ± 2[a]	84 ± 2[a,b]
Washed	Shore D hardness	78 ± 4[a]	79 ± 5[a]	81 ± 2[a]
	Weight change (%)	+0.57 ± 0.02[A]	+0.50 ± 0.03[A]*	+0.54 ± 0.05[A]
Washed and Dried	Shore D hardness	84 ± 3[a]	80 ± 4[a]	85 ± 2[b]
	Weight change (%)	−0.11 ± 0.01[B]	−0.13 ± 0.02[B]	−0.11 ± 0.01[B]

[a]Vertically, groups with identical small letters were not significantly different ($p > 0.05$) in hardness. Groups with identical capital letters were not significantly different ($p > 0.05$) in weight change. Horizontally, * means significantly different ($p < 0.05$) taking R as a reference.

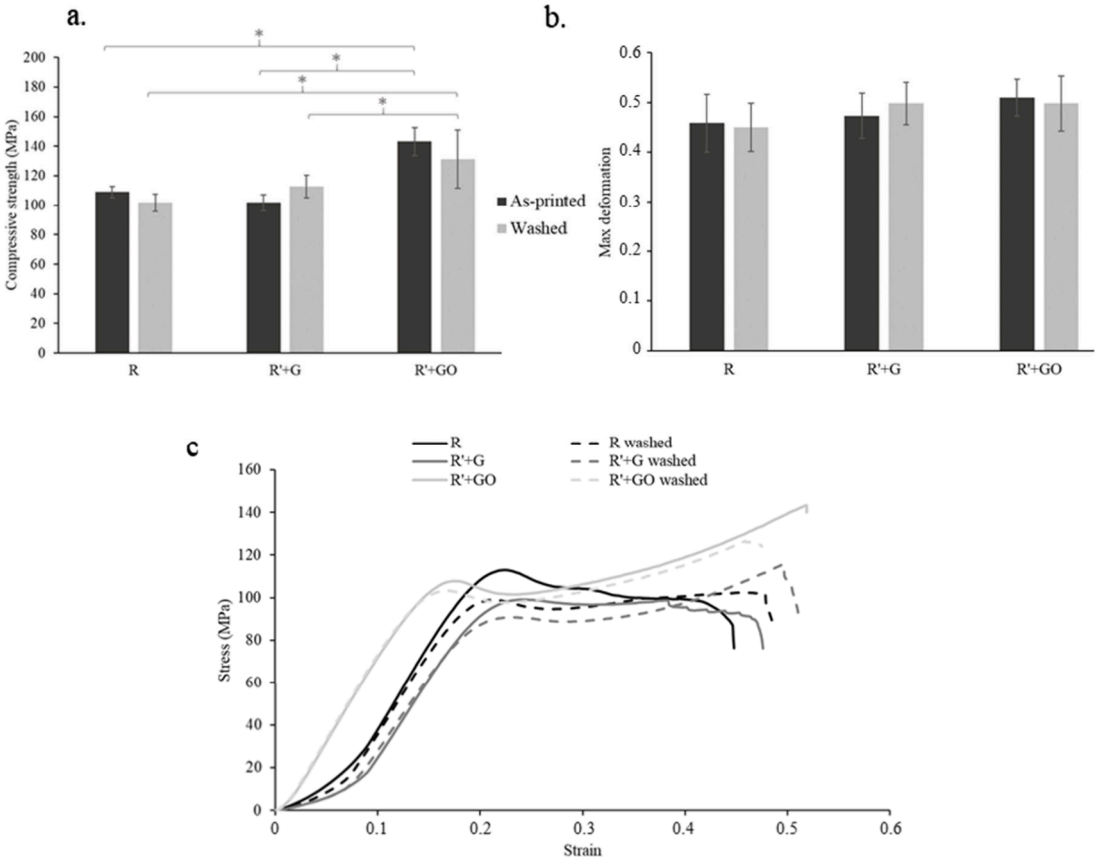

Figure 7. Compression tests for the base and GBN resins including (a) strength, (b) maximum deformation, and (c) characteristic stress−strain curves. * Means significantly different ($p < 0.05$).

washed twice. Nonetheless, the filler's nature remains a critical factor, with the addition of GO demonstrating the potential to elevate cellular performance to that of the washed native resin.

In light of these findings, twice-washed samples were treated with basal media, and eluents were collected after 7 days. Cultured cells after 1, 3, and 7 days showed a reduced presence of damaged cell membranes with a general increase in population across all samples over the 48 h and 7 days of incubation, with ∼100% of cell viability for all the samples (Figure 5). This shows that toxic compounds present in the resin can be effectively removed from the base resin and the nanocomposite samples through pretreatment in nutrient media.

To determine the nature of the released components responsible for the cytotoxic behavior of the eluents, ^{1}H NMR spectra were obtained.

^{1}H NMR spectra of the unwashed samples (Figure 6) showed small peaks at approximately 6.7 ppm, corresponding to the aromatic protons region, which, taking into account the resin composition, suggests the presence of the TPO photoinitiator. Conversely, the peaks observed at 3.7−3.8 ppm can be ascribed to the residual monomer, still noticeable in all conditions tested. When comparing each treatment, it was found that the R' samples showed an overall increase in peak intensity, suggesting that the addition of MMA led to a slightly higher amount of residual monomer and TPO release. More importantly, all aforementioned peaks disappeared when the samples were washed twice for 24 h. Therefore, the majority of the residual monomer and photoinitiator have been removed through the washing procedure, which could explain the increased cell viability (Figure 5).

To confirm if the residual monomer and photoinitiator were released, Shore D hardness and weight change were measured (Table 1). It was found that the presence of water in the polymer network produced a plasticization effect, reducing the surface hardness of the sample. This plasticization is caused by the separation of the polymer chains due to the presence of a water molecule, which does not form primary chemical bonds

https://doi.org/10.1021/acsomega.5c11858
ACS Omega 2026, 11, 20489−20499

with the polymer chain.[37] However, when water was desorbed, a decrease in weight accompanied by an increase in hardness was found in all cases suggesting that some components, i.e., residual monomer and photoinitiator, were removed.[34] These changes were only significant ($p > 0.05$) for R′ + GO.

3.2. Mechanical Properties

From stress−strain curves, compressive strength and the maximum deformation of the samples were calculated (Figure 7). For the as-printed samples, the addition of G did not change the compression strength from the base resin, while loading with GO led to a 30% increase. When comparing as-printed and washed samples, the washing process reduced the compression strength in R and R′ + GO samples (−6.7% and −8.3%, respectively) while increasing it in the case of R′ + G (+10.7%). However, differences between as-printed and washed samples are not significant in any case ($p > 0.05$). In the case of maximum deformation, differences between samples and post-treatments are very negligible ($p > 0.05$). These similarities can be observed in the stress−strain curves analyzed through UNE-EN ISO 604 with all samples demonstrating catastrophic failure (Figure 7c). Compression tests also provided information regarding the material toughness by analyzing the area under the curve. The stress−strain curve of GO (Figure 7c) shows a higher Young's modulus, compression strength and maximum strain than the other materials. Therefore, the addition of GO increases this toughness to a larger extent than the compression strength. Again, G did not change this parameter.

3.3. Weibull Analysis

Table 2 presents the results of the Weibull analysis for each experimental group, including the estimated Weibull parameters and their corresponding confidence intervals. Specifically, the table summarized the characteristic compressive strength (σ_θ) defined as the stress level at which 63.2% of the samples are expected to fail and the Weibull modulus (m), which reflects the variability of the strength values within each group.

Table 2. Weibull Parameters: Characteristic Compressive Strength (σ_θ), Weibull Modulus (m), and Their 95% Confidence Intervals (95% CI) for As-Printed and Washed Samples

		R	R′ + G	R′ + GO
As-printed	σ_θ (MPa)	110.7	108.0	149.0
	(95% CI)	(109.1−113.1)	(101.8−117.0)	(141.9−160.0)
	m	36.7	9.2	11.5
	(95% CI)	(7.8−65.7)	(2.5−15.8)	(2.42−20.5)
Washed	σ_θ (MPa)	104.4	118.3	143.7
	(95% CI)	(101.2−109.2)	(111.9−127.6)	(131−163.1)
	m	16.8	9.7	5.8
	(95% CI)	(4.5−29.0)	(2.6−16.8)	(1.6−10.0)

Figure 8 illustrates the cumulative probability of failure as a function of compressive strength for all studied groups. The dotted lines represent the theoretical Weibull distributions fitted to the data using the MLE method, while the individual data points correspond to the empirical failure probabilities of each experimental data calculated using the Hazen approximation. This combined representation provides a clear visual comparison between the experimental results and the fitted model, offering insight into the goodness of fit for each material group. In this context, lower Weibull modulus (m) values are associated with increased scatter in the experimental data, which is reflected by a larger dispersion of the data points around the theoretical Weibull distribution.

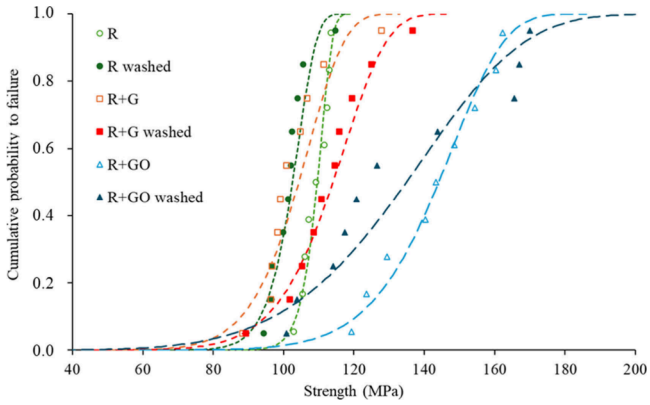

Figure 8. Cumulative probability of failure as a function of compressive strength derived from Weibull distribution for all materials (R, R′ + G, and R′ + GO) before and after washing.

The Weibull analysis reveals significant differences in the mechanical performance and reliability of the tested resins, both across material formulations and as a function of washing treatment.

The base resin (R) in the as-printed condition exhibited the lowest characteristic compressive strength (σ_θ = 110.7 MPa; 95% CI: 109.1−113.1 MPa), indicating reduced resistance to stress before failure. However, it showed the highest Weibull modulus (m = 36.7; 95% CI: 7.8−65.7), reflecting minimal variability and high consistency in mechanical performance. This indicates that the failure strengths for R were tightly clustered around the characteristic value.

In contrast, the graphene oxide-modified resin (R′ + GO) showed a substantially higher characteristic strength in the as-printed condition (σ_θ = 149.0 MPa; 95% CI: 141.9−160.0 MPa), clearly above the upper limit of the confidence interval for R, suggesting a statistically significant improvement in mechanical strength. However, the modulus decreased to m = 11.5 (CI: 2.4−20.5), indicating greater dispersion in the failure data.

The R′ + G resin exhibited a lower σ_θ than the formulation reinforced with GO, and a m that partially overlaps with both R and R′ + GO, suggesting that its performance is intermediate and not significantly distinct from the others in terms of variability.

These trends are also reflected in the cumulative probability of failure curves. At a compressive strength of 110 MPa, the probability of failure was approximately 40% for R, 70% for R′ + G, and only 5% for R′ + GO, underlining the reinforcement effect due to the addition of GO in enhancing strength and lowering failure probability.

Washing altered the mechanical performance of all resins, generally reducing their characteristic strength and reliability. This was reflected in downward shifts in the Weibull parameters and increased failure probabilities across all groups. The reduction in the m parameter after washing indicates greater data dispersion and decreased consistency in mechanical behavior. These trends suggest that washing may affect the internal structure or surface integrity of the resin, possibly by removing unreacted components or inducing microstructural changes, ultimately leading to reduced predictability in failure behavior.

https://doi.org/10.1021/acsomega.5c11858
ACS Omega 2026, 11, 20489−20499

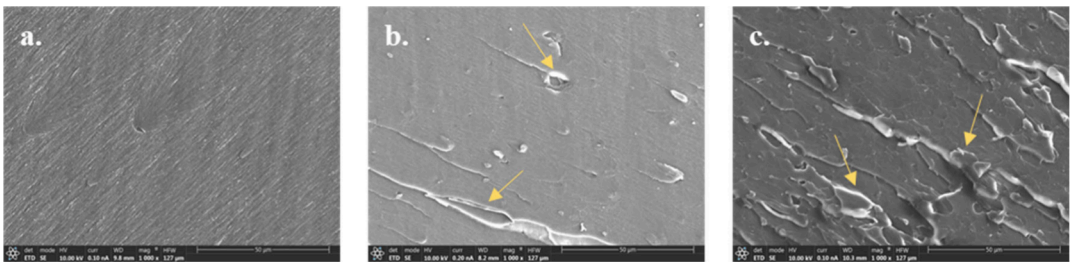

Figure 9. SEM micrographs of cryogenic fracture of (a) R, (b) R′ + G, and (c) R′ + GO (scale bar 50 μm).

These results highlight the trade-offs between mechanical strength and reliability in resin composites. While GO inclusion clearly improves strength, its associated variability, as seen in the reduced m parameter, must be controlled for consistent performance. Moreover, washing resulted in a substantial decrease in characteristic strength and reliability across all groups. However, the washed R′ + GO formulation still exhibited higher strength and lower failure probability compared to the other washed resins, underscoring its mechanical advantage even after postprocessing.

3.4. Fracture Analysis

To better analyze the fracture mechanics of the base and reinforced composites, the resulting surfaces of cryogenic fracture were analyzed by SEM (Figure 9). For the base resin (Figure 9a), a clean, smooth surface displaying a river-like pattern can be observed, with clear characteristics associated with brittle fractures.[35,38] However, the addition of GO (Figure 9c) has led to a series of multileveled features, accompanied by the significant presence of tortuous cracks and tear ridges. These observations strongly suggest instances of crack deflection and matrix/filler debonding within the material.[39] On the other hand, R′ + G (Figure 9b) presents a notably smoother surface, which may arise from the reduced entanglement or interlocking of polymer chains with the nanofiller particles. In addition, the presence of deep dimples likely indicates the aggregation of G, serving as a clear indicator of the nonuniform dispersion of G within the acrylic matrix.[40]

4. DISCUSSION

The results of the indirect cytotoxicity tests on the as-printed samples clearly indicate that the extracts from unwashed samples exhibited cytotoxic behavior, in agreement with previous observations from Xu et al.[41] on acrylic resin and the importance of washing to limit toxicity. Previous studies have explored different methods to reduce this cytotoxic effect by reducing the amount of residual monomer through rinsing in IPA,[41] water[26] or autoclaving.[28] In our experiments, washing the 3D-printed materials twice for 24 h each proved to be an effective method for enhancing their biocompatibility. According to ISO 10993-5, in vitro cytotoxicity may be assessed using extract-based methods to evaluate the biological effects of leachable substances released from a material. Within this regulatory framework, a material is considered non-cytotoxic when cell viability remains above 70% relative to the negative control. In this study, all washed samples tested using the extract-based approach exhibited cell viability values exceeding this threshold, confirming that the washing procedure effectively reduced the cytotoxic potential associated with residual monomers and photoinitiator-related species released from the printed resins.

NMR analysis indicated that the potentially toxic components, MMA and TPO, were either removed or no longer released into the media following this treatment. Previous researchers[42,43] have indicated a clear relationship between residual monomer and hardness with the residual monomer acting as a plasticizer, reducing hardness and rigidity. Although the effect is subtle due to the low amount of residual monomer and photoinitiator, the presented results support a reduction in weight and an increase in hardness after washing in basal media, suggesting the release of residual photoinitiator and monomer.

Based on the results of this study, the addition of MMA, employed as a strategy to achieve adequate dispersion of GBN in the polymer matrix, did not significantly impact cytotoxicity. However, it resulted in higher peak intensities in the NMR spectra, indicating a slightly increased release of residual components. Previous studies[44] proved that an increase in the amount of monomer in the formulation of acrylic resins results in a decrease on degree of conversion and, therefore, an increase in residual monomer. Consequently, the higher peak intensities can be due to a higher amount of residual monomer when adding MMA to the resin. Regarding the nanocomposites with GBN, interestingly, R′ + G required additional washes to achieve biocompatibility levels comparable to R′ + GO. Despite these differences, all washed samples demonstrated cell viability above 90%, indicating that with proper washing protocols, these materials can be considered biocompatible for biomedical applications.

The higher toxicity observed in G is likely attributed to the increased presence of residual monomers and photoinitiators, resulting from the lower degree of polymerization in R′ + G, as reported by previous studies,[32] where an inhibition of the polymerization process was found due to the presence of G. This lower degree of polymerization was also observed in the reduction of double bond conversion (DBC) found in previous studies when G was added to the resin.[45]

In terms of mechanical properties, the addition of GO increased compressive strength by 30%, whereas G did not produce significant improvements. The influence of G and GO on mechanical performance stems from their ability to deflect crack fronts and hinder crack propagation, effects that are more pronounced in terms of toughness and dynamic loading rather than static mechanical strength.[12] In this study, the addition of GO significantly increased the area under the compression test curve, indicating enhanced toughness in the nanocomposite. Achieving such improvements with nanofillers requires good dispersion within the polymer matrix and strong interfacial adhesion, as widely documented.[46,47] The interaction between GO and the matrix confirmed through SEM analysis, demonstrated effective bonding that contributed to these enhancements. In contrast, the lack of mechanical improve-

https://doi.org/10.1021/acsomega.5c11858
ACS Omega 2026, 11, 20489−20499

ment with G is attributed to poor adhesion between the nanographene filler and the resin, resulting in diminished mechanical performance, as previously found by Hanon et al.[48] when using graphene as a filler in a biobased photocurable resin.

The use of Weibull analysis in this study aligns with its proven utility in evaluating the mechanical reliability of materials for orthopedic and tissue engineering applications. Previous studies, such as Prakash et al.,[30] demonstrated the effectiveness of Weibull distribution for assessing the reliability of 3D-printed PLA/HA scaffolds, highlighting its relevance for tissue engineering and biomedical applications. Similarly, Barui et al.[31] applied Weibull analysis to 3D-printed Ti-6Al-4 V biomaterials, emphasizing its importance in evaluating the strength reliability of orthopedic implants. These studies validate the application of Weibull analysis as a robust tool for assessing variability and predictability in mechanical performance, providing a deeper understanding of the material's suitability for load-bearing and long-term biomedical applications.

The Weibull analysis proved essential for complementing traditional mechanical testing, offering insight not only into average material strength but also into the reliability and consistency of performance. While GO-modified resins reached characteristic strength values (σ_θ) within the range reported for cortical bone (130 and 200 MPa).[49] Their lower Weibull moduli revealed higher variability in failure behavior. This variability may limit their applicability in scenarios requiring predictable mechanical responses. In contrast, the base resin (R), despite its lower strength, demonstrated superior reliability through a higher m value. These findings highlight the critical role of Weibull statistics in identifying trade-offs between strength and reliability—information that remains hidden in conventional average-based analysis. For biomedical applications, where both high strength and consistent performance are required, such dual-parameter evaluation becomes a key decision-making tool.

The findings from this study highlight the importance of such evaluations, demonstrating that understanding and addressing variability are as critical as improving mechanical performance when developing materials for prosthetics, scaffolds, and other biomedical products. In addition, a preliminary cost estimation was performed for the best-performing formulation (R′ + GO), indicating that the incorporation of graphene oxide leads to an approximate 14% increase in material cost compared to the neat commercial resin (R). Although this represents a moderate rise in production expenses, it may still be justified in biomedical applications, where material selection is primarily driven by mechanical performance, reliability, and functional benefits rather than purely cost-minimization, supporting the potential feasibility of the proposed formulation for specialized clinical and research-oriented uses.

5. CONCLUSIONS

Based on the study findings, the photocurable acrylic resins studied here, including those modified with graphene (G) and graphene oxide (GO), exhibit sufficient biocompatibility and mechanical reliability for biomedical applications when subjected to an appropriate washing protocol. These attributes are particularly important for biomedical products, where consistent and predictable performance under mechanical stress is essential to ensure patient safety and functionality. The washing process achieved cell viability above 90%, confirming the safety of these materials for extended interaction with the human body.

GO-modified resins showed a marked improvement in mechanical strength, with increases observed in both the maximum compression strength and the characteristic strength (σ_θ) compared to the base resin (R). However, Weibull analysis showed that GO-modified resins exhibited slightly greater variability in mechanical performance compared to R, indicating differences in reliability. While G-modified resins did not enhance mechanical strength significantly, they maintained reliability comparable to the base resin.

This study highlights the potential of stereolithography as a versatile platform for fabricating intricate, biocompatible, and mechanically reliable materials for biomedical applications, such as prostheses and scaffolds. GO-modified resins offer a combination of enhanced mechanical performance and biocompatibility, paving the way for their use in biomedical applications where product safety and reliability are paramount. However, the slightly lower predictability in mechanical performance observed with GO-modified resins suggests that further evaluation may be necessary to ensure consistent performance under diverse biomedical conditions.

AUTHOR INFORMATION

Corresponding Author

Sara Lopez de Armentia − *Institute for Research in Technology/Mechanical Engineering Department, Universidad Pontificia Comillas, 28015 Madrid, Spain;* orcid.org/0000-0002-5460-9132; Email: sara.lopez@comillas.edu

Authors

Victor Manuel Villapún − *School of Chemical Engineering, University of Birmingham, Edgbaston B15 2TT, United Kingdom;* orcid.org/0000-0001-6400-528X

Yolanda Ballesteros − *Institute for Research in Technology/Mechanical Engineering Department, Universidad Pontificia Comillas, 28015 Madrid, Spain;* orcid.org/0000-0001-9023-721X

Juan Carlos del Real − *Institute for Research in Technology/Mechanical Engineering Department, Universidad Pontificia Comillas, 28015 Madrid, Spain*

Lucy Arkinstall − *School of Chemical Engineering, University of Birmingham, Edgbaston B15 2TT, United Kingdom*

Sophie Constance Cox − *School of Chemical Engineering, University of Birmingham, Edgbaston B15 2TT, United Kingdom*

Nicholas Dunne − *Centre for Medical Engineering Research, School of Mechanical and Manufacturing Engineering, Dublin City University, Dublin 9, Ireland; School of Mechanical and Manufacturing Engineering, Centre for Medical Engineering Research, School of Mechanical and Manufacturing Engineering, and Advanced Processing Technology Research Centre, Dublin City University, Dublin 9, Ireland; School of Pharmacy, Queen's University of Belfast, Belfast BT9 7BL, U.K.; Department of Mechanical and Manufacturing Engineering, School of Engineering, Advanced Materials and Bioengineering Research Centre (AMBER), and Trinity Centre for Biomedical Engineering, Trinity Biomedical Sciences Institute, Trinity College Dublin, Dublin 2, Ireland; Advanced Manufacturing Research Centre (I-*

https://doi.org/10.1021/acsomega.5c11858
ACS Omega 2026, 11, 20489−20499

Form), School of Mechanical and Manufacturing Engineering, Dublin City University, Dublin 9, Ireland
Eva Paz − *Institute for Research in Technology/Mechanical Engineering Department, Universidad Pontificia Comillas, 28015 Madrid, Spain;* orcid.org/0000-0002-7440-8995

Complete contact information is available at: https://pubs.acs.org/10.1021/acsomega.5c11858

Funding

This work was supported by Comillas Pontifical University (grant number PP2024_33).

Notes

The authors declare no competing financial interest.

REFERENCES

(1) Prpic, V.; Slacanin, I.; Schauperl, Z.; Catic, A.; Dulcic, N.; Cimic, S. A Study of the Flexural Strength and Surface Hardness of Different Materials and Technologies for Occlusal Device Fabrication. *J. Prosthet. Dent.* **2019**, *121* (6), 955−959.
(2) Albahri, R.; Yoon, H. I.; Lee, J. D.; Yoon, S.; Lee, S. J. Shear Bond Strength of Provisional Repair Materials Bonded to 3D Printed Resin. *J. Dent. Sci.* **2021**, *16* (1), 261−267.
(3) Da Silva, T. M.; Immich, F.; De Araujo, T. S.; Lund, R. G.; Da Silva, A. F.; Piva, E.; Da Rosa, W. L. D. O. Photosensitive Resins Used in Additive Manufacturing for Oral Application in Dentistry: A Scoping Review from Lab to Clinic. *J. Mech. Behav. Biomed. Mater.* **2023**, *141*, 105732.
(4) Kanwar, S.; Vijayavenkataraman, S. Design of 3D Printed Scaffolds for Bone Tissue Engineering: A Review. *Bioprinting* **2021**, *24*, No. e00167.
(5) Zhang, Y.; Zhang, Q.; He, F.; Zuo, F.; Shi, X. Fabrication of Cancellous-Bone-Mimicking β-Tricalcium Phosphate Bioceramic Scaffolds with Tunable Architecture and Mechanical Strength by Stereolithography 3D Printing. *J. Eur. Ceram. Soc.* **2022**, *42* (14), 6713−6720.
(6) Baino, F.; Magnaterra, G.; Fiume, E.; Schiavi, A.; Tofan, L. P.; Schwentenwein, M.; Verné, E. Digital Light Processing Stereolithography of Hydroxyapatite Scaffolds with Bone-like Architecture, Permeability, and Mechanical Properties. *J. Am. Ceram. Soc.* **2022**, *105* (3), 1648−1657.
(7) Lopez de Armentia, S.; del Real, J. C.; Paz, E.; Dunne, N. Advances in Biodegradable 3D Printed Scaffolds with Carbon-Based Nanomaterials for Bone Regeneration. *Materials* **2020**, *13* (22), 5083.
(8) Schmidleithner, C.; Kalaskar, D. M. Stereolithography. In *3D Printing*; InTech, 2018; pp 3−22. DOI: 10.5772/intechopen.78147.
(9) Murphy, C. M.; Haugh, M. G.; O'Brien, F. J. The Effect of Mean Pore Size on Cell Attachment, Proliferation and Migration in Collagen-Glycosaminoglycan Scaffolds for Bone Tissue Engineering. *Biomaterials* **2010**, *31*, 461−466.
(10) Yang, S.; Leong, K.-F.; Du, Z. M. E.; Chua, C.-K. The Design of Scaffolds for Use in Tissue Engineering. Part I. Traditional Factors. *Tissue Eng.* **2001**, *7* (6), 679−689.
(11) Murphy, C. M.; O'Brien, F. J. Understanding the Effect of Mean Pore Size on Cell Activity in Collagen-Glycosaminoglycan Scaffolds. *Cell Adh. Migr.* **2010**, *4* (3), 377−381.
(12) Paz, E.; Forriol, F.; del Real, J. C.; Dunne, N. Graphene Oxide versus Graphene for Optimisation of PMMA Bone Cement for Orthopaedic Applications. *Materials Science and Engineering C* **2017**, *77*, 1003−1011.
(13) Tavakoli, M.; Bakhtiari, S. S. E.; Karbasi, S. Incorporation of Chitosan/Graphene Oxide Nanocomposite in to the PMMA Bone Cement: Physical, Mechanical and Biological Evaluation. *Int. J. Biol. Macromol.* **2020**, *149*, 783−793.
(14) Malik, S.; Ruddock, F. M.; Dowling, A. H.; Byrne, K.; Schmitt, W.; Khalakhan, I.; Nemoto, Y.; Guo, H.; Shrestha, L. K.; Ariga, K.; Hill, J. P. Graphene Composites with Dental and Biomedical Applicability. *Beilstein Journal of Nanotechnology* **2018**, *9* (1), 801−808.
(15) Aryaei, A.; Jayatissa, A. H.; Jayasuriya, A. C. The Effect of Graphene Substrate on Osteoblast Cell Adhesion and Proliferation. *J. Biomed. Mater. Res., Part A* **2014**, *102* (9), 3282−3290.
(16) Wang, W.; Junior, J. R. P.; Nalesso, P. R. L.; Musson, D.; Cornish, J.; Mendonça, F.; Caetano, G. F.; Bártolo, P. Engineered 3D Printed Poly(ε-Caprolactone)/Graphene Scaffolds for Bone Tissue Engineering. *Materials Science and Engineering C* **2019**, *100*, 759−770.
(17) Eivazzadeh-Keihan, R.; Maleki, A.; de la Guardia, M.; Bani, M. S.; Chenab, K. K.; Pashazadeh-Panahi, P.; Baradaran, B.; Mokhtarzadeh, A.; Hamblin, M. R. Carbon Based Nanomaterials for Tissue Engineering of Bone: Building New Bone on Small Black Scaffolds: A Review. *J. Adv. Res.* **2019**, *18*, 185−201.
(18) Teimoorian, M.; Mirzaie, M.; Tashakkorian, H.; Gholinia, H.; Alaghemand, H.; Pournajaf, A.; Ghorbanipour, R. Effects of Adding Functionalized Graphene Oxide Nanosheets on Physical, Mechanical, and Anti-Biofilm Properties of Acrylic Resin: In Vitro-Experimental Study. *Dent. Res. J. (Isfahan).* **2023**, *20* (1), PMC10166752.
(19) Aati, S.; Chauhan, A.; Shrestha, B.; Rajan, S. M.; Aati, H.; Fawzy, A. Development of 3D Printed Dental Resin Nanocomposite with Graphene Nanoplatelets Enhanced Mechanical Properties and Induced Drug-Free Antimicrobial Activity. *Dental Materials* **2022**, *38* (12), 1921−1933.
(20) MacDonald, A. F.; Harley-Troxell, M. E.; Newby, S. D.; Dhar, M. S. 3D-Printing Graphene Scaffolds for Bone Tissue Engineering. *Pharmaceutics* **2022**, *14*, 1834.
(21) Raszewski, Z. Influence of Polymerization Method on the Cytotoxicity of Three Different Denture Base Acrylic Resins Polymerized in Different Methods. *Saudi J. Biol. Sci.* **2020**, *27* (10), 2612−2616.
(22) Li, P.; Lambart, A. L.; Stawarczyk, B.; Reymus, M.; Spintzyk, S. Postpolymerization of a 3D-Printed Denture Base Polymer: Impact of Post-Curing Methods on Surface Characteristics, Flexural Strength, and Cytotoxicity. *J. Dent.* **2021**, *115*, 103856.
(23) Formlabs. *3D Printing Materials For Healthcare*. https://formlabs.com/materials/medical/ (accessed 2023−11−17).
(24) Jeršovaitė, J.; Šarachovaitė, U.; Matulaitienė, I.; Niaura, G.; Baltriukienė, D.; Malinauskas, M. Biocompatibility Enhancement via Post-Processing of Microporous Scaffolds Made by Optical 3D Printer. *Front. Bioeng. Biotechnol.* **2023**, *11*, 1167753.
(25) Bural, C.; Aktas, E.; Deniz, G.; Ünlüçerçi, Y.; Kizilcan, N.; Bayraktar, G. Effect of Post-Polymerization Heat-Treatments on Degree of Conversion, Leaching Residual MMA and in Vitro Cytotoxicity of Autopolymerizing Acrylic Repair Resin. *Dental Materials* **2011**, *27* (11), 1135−1143.
(26) Sheridan, P. J.; Koka, S.; Ewoldsen, N. O.; Lefebvre, C. A.; Lavin, M. T. Cytotoxicity of Denture Base Resins. *Int. J. Prosthodont.* **1997**, *10* (1), 73−77.
(27) Urban, V. M.; Machado, A. L.; Oliveira, R. V.; Vergani, C. E.; Pavarina, A. C.; Cass, Q. B. Residual Monomer of Reline Acrylic Resins. Effect of Water-Bath and Microwave Post-Polymerization Treatments. *Dental Materials* **2007**, *23*, 363−368.
(28) Tangpothitham, S.; Pongprueksa, P.; Inokoshi, M.; Mitrirattanakul, S. Effect of Post-Polymerization with Autoclaving Treatment on Monomer Elution and Mechanical Properties of 3D-Printing Acrylic Resin for Splint Fabrication. *J. Mech. Behav. Biomed. Mater.* **2022**, *126*, 105015.
(29) Oskui, S. M.; Diamante, G.; Liao, C.; Shi, W.; Gan, J.; Schlenk, D.; Grover, W. H. Assessing and Reducing the Toxicity of 3D-Printed Parts. *Environ. Sci. Technol. Lett.* **2016**, *3* (1), 1−6.
(30) Prakash, C.; Singh, G.; Singh, S.; Linda, W. L.; Zheng, H. Y.; Ramakrishna, S.; Narayan, R. Mechanical Reliability and In Vitro Bioactivity of 3D-Printed Porous Polylactic Acid-Hydroxyapatite Scaffold. *J. Mater. Eng. Perform.* **2021**, *30* (7), 4946−4956.
(31) Barui, S.; Panda, A. K.; Naskar, S.; Kuppuraj, R.; Basu, S.; Basu, B. 3D Inkjet Printing of Biomaterials with Strength Reliability and Cytocompatibility: Quantitative Process Strategy for Ti-6Al-4V. *Biomaterials* **2019**, *213*, 119212.

(32) Lopez de Armentia, S.; Abenojar, J.; Ballesteros, Y.; del Real, J. C.; Dunne, N.; Paz, E. Polymerization Kinetics of Acrylic Photopolymer Loaded with Graphene-Based Nanomaterials for Additive Manufacturing. *Nanomaterials* **2022**, *12* (24), 4498.
(33) de Armentia, S. L.; Fernández-Villamarín, S.; Ballesteros, Y.; del Real, J. C.; Dunne, N.; Paz, E. 3D Printing of a Graphene-Modified Photopolymer Using Stereolithography for Biomedical Applications: A Study of the Polymerization Reaction. *Int. J. Bioprint.* **2022**, *8* (1), 503.
(34) Urban, V. M.; Machado, A. L.; Vergani, C. E.; Giampaolo, E. T.; Pavarina, A. C.; de Almeida, F. G.; Cass, Q. B. Effect of Water-Bath Post-Polymerization on the Mechanical Properties, Degree of Conversion, and Leaching of Residual Compounds of Hard Chairside Reline Resins. *Dental Materials* **2009**, *25* (5), 662−671.
(35) Hussein, A.; Sarkar, S.; Lee, K.; Kim, B. Cryogenic Fracture Behavior of Epoxy Reinforced by a Novel Graphene Oxide/Poly(p-Phenylenediamine) Hybrid. *Compos. B Eng.* **2017**, *129*, 133−142.
(36) Virtanen, P.; Gommers, R.; Oliphant, T. E.; Haberland, M.; Reddy, T.; Cournapeau, D.; Burovski, E.; Peterson, P.; Weckesser, W.; Bright, J.; van der Walt, S. J.; Brett, M.; Wilson, J.; Millman, K. J.; Mayorov, N.; Nelson, A. R. J.; Jones, E.; Kern, R.; Larson, E.; Carey, C. J.; Polat, İ.; Feng, Y.; Moore, E. W.; VanderPlas, J.; Laxalde, D.; Perktold, J.; Cimrman, R.; Henriksen, I.; Quintero, E. A.; Harris, C. R.; Archibald, A. M.; Ribeiro, A. H.; Pedregosa, F.; van Mulbregt, P.; Vijaykumar, A.; Bardelli, A. P.; Rothberg, A.; Hilboll, A.; Kloeckner, A.; Scopatz, A.; Lee, A.; Rokem, A.; Woods, C. N.; Fulton, C.; Masson, C.; Häggström, C.; Fitzgerald, C.; Nicholson, D. A.; Hagen, D. R.; Pasechnik, D. V.; Olivetti, E.; Martin, E.; Wieser, E.; Silva, F.; Lenders, F.; Wilhelm, F.; Young, G.; Price, G. A.; Ingold, G. L.; Allen, G. E.; Lee, G. R.; Audren, H.; Probst, I.; Dietrich, J. P.; Silterra, J.; Webber, J. T.; Slavič, J.; Nothman, J.; Buchner, J.; Kulick, J.; Schönberger, J. L.; de Miranda Cardoso, J. V.; Reimer, J.; Harrington, J.; Rodríguez, J. L. C.; Nunez-Iglesias, J.; Kuczynski, J.; Tritz, K.; Thoma, M.; Newville, M.; Kümmerer, M.; Bolingbroke, M.; Tartre, M.; Pak, M.; Smith, N. J.; Nowaczyk, N.; Shebanov, N.; Pavlyk, O.; Brodtkorb, P. A.; Lee, P.; McGibbon, R. T.; Feldbauer, R.; Lewis, S.; Tygier, S.; Sievert, S.; Vigna, S.; Peterson, S.; More, S.; Pudlik, T.; Oshima, T.; Pingel, T. J.; Robitaille, T. P.; Spura, T.; Jones, T. R.; Cera, T.; Leslie, T.; Zito, T.; Krauss, T.; Upadhyay, U.; Halchenko, Y. O.; Vázquez-Baeza, Y. SciPy 1.0: Fundamental Algorithms for Scientific Computing in Python. *Nat. Methods* **2020**, *17*, 261−272.
(37) Medeiros, I. S.; Gomes, M. N.; Loguercio, A. D.; Filho, L. E. R. Diametral Tensile Strength and Vickers Hardness of a Composite after Storage in Different Solutions. *J. Oral Sci.* **2007**, *49* (1), 61−66.
(38) Olowojoba, G. B.; Eslava, S.; Gutierrez, E. S.; Kinloch, A. J.; Mattevi, C.; Rocha, V. G.; Taylor, A. C. In Situ Thermally Reduced Graphene Oxide/Epoxy Composites: Thermal and Mechanical Properties. *Applied Nanoscience (Switzerland)* **2016**, *6* (7), 1015−1022.
(39) Fan, J.; Yang, J.; Li, H.; Tian, J.; Wang, M.; Zhao, Y. Cryogenic Mechanical Properties of Graphene Oxide/Epoxy Nanocomposites: Influence of Graphene Oxide with Different Oxidation Degrees. *Polym. Test.* **2021**, *96*, 107074.
(40) Sekhavat Pour, Z.; Ghaemy, M. Polymer Grafted Graphene Oxide: For Improved Dispersion in Epoxy Resin and Enhancement of Mechanical Properties of Nanocomposite. *Compos. Sci. Technol.* **2016**, *136*, 145−157.
(41) Xu, Y.; Xepapadeas, A. B.; Koos, B.; Geis-Gerstorfer, J.; Li, P.; Spintzyk, S. Effect of Post-Rinsing Time on the Mechanical Strength and Cytotoxicity of a 3D Printed Orthodontic Splint Material. *Dental* **2021**, *37*, No. e314.
(42) Lee, S. Y.; Lai, Y. L.; Hsu, T. S. Influence of Polymerization Conditions on Monomer Elution and Microhardness of Autopolymerized Polymethyl Methacrylate Resin. *Eur. J. Oral Sci.* **2002**, *110* (2), 179−183.
(43) fawzy, a.; Abdelrahim, R.; Abdel Hameed, B. Assessment of Hardness, Flexural Modulus, and Bond Strength of Acrylic Denture Bases Fabricated by 3D Digital Methods. *Egypt. Dent. J.* **2021**, *67* (3), 2559−2566.
(44) Hata, K.; Ikeda, H.; Nagamatsu, Y.; Masaki, C.; Hosokawa, R.; Shimizu, H. Development of Dental Poly(Methyl Methacrylate)-Based Resin for Stereolithography Additive Manufacturing. *Polymers (Basel).* **2021**, *13* (24), 4435.
(45) de Armentia, S. L.; Giménez, R.; del Real, J. C.; Serrano, B.; Cabanelas, J. C.; Paz, E. Effect of Graphene and Graphene Oxide Addition on Crosslinking and Mechanical Properties of Photocurable Resins for Stereolithography. *Int. J. Bioprint.* **2024**, *10* (6), 194−208.
(46) Shuai, C.; Guo, W.; Wu, P.; Yang, W.; Hu, S.; Xia, Y.; Feng, P. A Graphene Oxide-Ag Co-Dispersing Nanosystem: Dual Synergistic Effects on Antibacterial Activities and Mechanical Properties of Polymer Scaffolds. *Chemical Engineering Journal* **2018**, *347*, 322−333.
(47) Paz, E.; Ballesteros, Y.; Abenojar, J.; Dunne, N.; Del Real, J. C. Advanced G-MPS-PMMA Bone Cements: Influence of Graphene Silanisation on Fatigue Performance, Thermal Properties and Biocompatibility. *Nanomaterials* **2021**, *11* (1), 139.
(48) Hanon, M. M.; Ghaly, A.; Zsidai, L.; Szakál, Z.; Szabó, I.; Kátai, L. Investigations of the Mechanical Properties of Dlp 3d Printed Graphene/Resin Composites. *Acta Polytechnica Hungarica* **2021**, *18* (8), 143−161.
(49) Gerhardt, L. C.; Boccaccini, A. R. Bioactive Glass and Glass-Ceramic Scaffolds for Bone Tissue Engineering. *Materials* **2010**, *3*, 3867−3910.

https://doi.org/10.1021/acsomega.5c11858
ACS Omega 2026, 11, 20489−20499